Development of Metamaterial-Based Biosensor for Biomedical Applications

A. H. Jabire[1*], S. Saminu[2], A. A. Owoade[3], D. A. Ariyoosu[3], A. M. Sadiq [4], M. J. Adamu[5] and M. I. Hussein[6]

[1]Department of Electrical and Electronics Engineering, Taraba State University, Jalingo, Nigeria.
[2]Department of Biomedical Engineering, University of Ilorin, Ilorin, Nigeria.
[3]Department of Islamic Law, University of Ilorin, Ilorin, Nigeria.
[4]Tianjin Key Laboratory of Imaging and Sensing Microelectronic Technology, School of Microelectronics, Tianjin University, Tianjin, 30072, China.
[5]Department of Electronic Science and Technology, School of Microelectronics, Tianjin University, China.
[6]Department of Electrical and Communication Engineering, United Arab Emirates University, AL-Ain, United Arab Emirate.

ABSTRACT: Breast cancer is one of the most commonly diagnosed cancers among women. For fast and effective treatment of breast cancer, early detection is inevitable. Material characterization or detection is essential for identifying the specific type of material suited for a given application, whether it is a solid, semi-solid, liquid, or powdered sample. This study presents a biosensor that utilizes metamaterials to detect cancerous cells through their electrical properties for clinical diagnostics. The design features a rectangular patch microstrip-fed grounded planar structure with a split ring resonator (SRR) loaded at two ports. The SRR is constructed utilizing its inductive and capacitive resonance characteristics, rendering it an appropriate sensing option. Using the four different breast cancer cells as material detection units and air as a reference, detection is performed. The evaluation of the sensor's performance involves the analysis of four distinct breast cancer cells: HS578, MCF-7, MDA-MB-231, and MDA-2. The RLC equivalent circuit has been introduced to enhance the comprehension of the sensor's functionality. The measurement outcomes of the prototype sensor aligned closely with simulated results derived from the computer simulation technology suite (CST) and Advanced design system (ADS). The biosensor can be suitably integrated into clinical diagnostic tools for the early detection and classification of breast cancer. This will potentially enable timely detection of cancer and precise treatment of breast cancer.

KEYWORDS: Biosensor, Equivalent circuit, Metamaterial, Split rectangular resonator, Sensitivity, Breast cancer detection

[Received Jan. 13, 2025; Revised Mar. 2, 2025; Accepted Mar. 8, 2025] Print ISSN: 0189-9546 | Online ISSN: 2437-2110

I. INTRODUCTION

Due to technological advancement and rapid software development, the trend toward non-invasive sensing and prognosis of chemical and medical material across various applications is increasing rapidly. The fast detection and diagnosis approach has attracted the attention of scientists and researchers in clinics, laboratories, food industries, security, and various other fields. Typically, the sensor includes a sensing component that can accurately define the properties of the material under test (MUT) (Yadav R. & Patel P. N., 2018) (Juan G. et al., 2019) through contact, immersion, or proximity. Microwave sensors find extensive application across multiple fields, including industrial, biological, and electronic sectors, owing to their significant benefits, such as high sensitivity, adaptability, cost-effectiveness in manufacturing, and ease of measurement. Microwave sensing fundamentally operates on the principles of band-pass filter technology; sensors that use resonators identify changes in the resonant frequency of a resonant component when a material under test (MUT) is placed on the surface of the resonator. The frequency response's amplitude and resonant frequency deviate from the original resonance frequency of the structure, influenced by the permittivity and thickness of the applied MUT. Structures based on planar resonators, engineered to function across a broad frequency range from microwave to terahertz (THz), are considered highly promising for a variety of sensing applications. Many researchers have investigated different microwave measurement techniques over the years to characterize the biological samples (Xinyue S., Sen Y., and Chen J., 2023) (Chuma E. I., Lano Y., Fontgallanad G., et al. 2018).

Each characterization technique depends on various factors, such as the sample properties and the frequency range used for the analysis (Carnerero-Cano J. et al., 2018). The waveguide (cavity) is one method employed by several researchers to study material properties (Galindo-Romero G. et al., 2017). The coaxial method represents a sophisticated, non-invasive technique that has been extensively developed. This approach is advantageous as it allows for the analysis of materials without necessitating their extraction from the organism. Measurements are conducted by positioning the open end of a coaxial line adjacent to the material of interest, enabling the determination of the material's dielectric properties through the analysis of the reflected signal. (Mousa I. Hussein, et al., 2019). Resonant microwave sensors, influenced by metamaterial designs, have become increasingly favoured within the realm of planar sensors, finding utility in

*Corresponding author: adamu.jabire@tsuniversity.edu.ng *doi:* http://dx.doi.org/10.4314/njtd.v22i1.3282

diverse applications, including the detection of oil impurities (Yahzmee P., and Minoofar H., 2014), humidity sensing (J. K.Park. Jang C. Yun G. H. et al. 2014), biosensing (Memon M. U. Salim A. Jeong H., et al. 2020), food adulteration detection (Varshney P. K. Sharma A., and Akhtar M. J. 2020), Microfluidic sensing (Su W. Cook B. S., and Tentzeris M. M. 2016), (Juan C.G, Bronchalo E. Potelon B., et al. 2019), (Withayachumnankul W. Jaruwongrungsee K., Tuantranont A., et al 2013), (Buragohain A. Mostako T. T., and Das G. S., 2021), permittivity measurements (Ansari M. A. H. Jha A. K., and Akhtar M. J., 2015), (Shafi M. K.T., Jha A. K., and Akhtar M. J., 2017), (Boybay M. S., and Ramahi O. M. 2012), and rotation sensing (Naqui J and Martin F. 2014).

Comprehensive studies in the literature have utilized different microwave sensor methods based on metamaterials (E. L. Chuma and T. Rasmussen, 2022) and introduced a sensor utilizing microwave and near-infrared metamaterials. The design uses a flat circular CSRR configuration. The microwave sensor identifies the adulteration of olive oil by using classification algorithms for training. A microwave sensor designed for the dielectric characterization of biological samples is presented by (G. Gugliandolo, G. Vermiglin, et al. 2023). The resonant configuration is made up of two capacitively linked printed SRRs created utilizing the inkjet printing method. In (E. L. Chuma, Y. Iano, L. L. B., et al., 2022), A sensor based on Complementary Split Ring Resonators (CSRR) has been developed for the detection of wear particles in lubricating oil. This innovative design incorporates neodymium magnets strategically positioned at the centre of the CSRR framework to attract particles with coloured coatings effectively. A key tool for characterizing microwave components is the equivalent circuit model, which clarifies the principles and operations of this research. This model has been extensively utilized in the analysis and modelling of radiating antennas. (Jabire A. H. et al, 2024). A dual-scale planar sensor for dielectric characterization of solid material was presented by (Hong X. San Y. et al, 2022). However, it has a good sensitivity, but it is lower than the one proposed, and the design is complex. A solid material permittivity characterization was reported in (K. Massakin, S. Z. Ibrahim, et al. 2023); the sensitivity is low compared to the one presented in this work.

The goal of this research is to use a high-sensitivity microwave sensor in order to categorize and distinguish different types of cancer cells according to their electrical properties. This investigation will focus on four specific cancer cell lines: HS578, MCF-7, MDA-MB-231, and MDA-2. The electrical properties of these cancerous cells were obtained from prior studies conducted by researchers in the field (D. Jithin, M. I. Hussein, et al. 2016). The letter consists of four sections. Section 2 offers a theoretical analysis. The microwave sensor design process, the proposed sensor configuration, and the equivalent circuit model are described in section 3. In section 4, the measured outcomes and the hardware prototype are examined. Section 5 provides the concluding remarks.

II. THEORETICAL ANALYSIS

Based on the idea of field interaction with the material under test (MUT), the suggested microwave sensor operates. The resonator's electromagnetic field is counteracted by polarization, which happens when a dielectric material is added. The polarization effect causes the dipoles' oscillation frequency inside the MUT to be delayed, which lowers the resonator frequency. A dielectric resonator's resonant frequency shifts to a lower value when a MUT is present, to put it another way. The MUT's complex permittivity directly affects how much of a shift this is. The resonance frequency shift increases with the permittivity value. Equation (1) explains this frequency shift (D. M. Pozar, 2017).

$$\frac{\Delta f_r}{f_r} = \frac{\int(\Delta\varepsilon E_s.E_0+\Delta\mu H_s.H_0)dv}{\int(\varepsilon_0.|E_0|^2+\mu_0.|H_0|^2)dv} \quad (1)$$

In this context, f_r denotes the frequency of resonance, where ε represents the permittivity and μ signifies the permeability. The variables E_0 and H_0 correspond to the electric and magnetic fields in a discharged state, respectively, while E_s and H_s indicate the fields observed in the presence of the material under test (MUT). The proposed sensor design also capitalizes on the SRR capacitive and inductive resonance properties. According to equation (2) (P. K. Varshney, A. Kapoor and M. J. Akhtar, 2021), (S. Jiang, G. Liu, M. Wang et al. 2023)

$$f = \frac{1}{2\pi\sqrt{L_{eff}C_{eff}}} \quad (2)$$

The terms L_{eff} and C_{eff} denote the effective inductance and capacitance associated with the resonator. (A. Ebrahimi, J. Scott and K. Ghorbani, 2018). Basically, the capacitance (C) is given by

$$C = \frac{\varepsilon_0\varepsilon_r A}{d} \quad (3)$$

The relative permittivity of vacuum is denoted as ε_0, while ε_r represents the relative permittivity of the dielectric material. The parameters A and d refer to the area of the gap and the distance of the gap, respectively. Given that ε_0, A, and d remain constant for a specific sample, the value of ε_r influences the capacitance. This value is contingent upon the unique ε_r associated with each cancer cell, which ultimately results in alterations to the frequency of resonance of the split-ring resonator (SRR).

III. METHODOLOGY

The proposed microwave sensor consists of a sensing patch arrangement that is activated by a two-port microstrip, as shown in Figure 1. The conductive ring carries current when a magnetic field interacts with the SRR, which is a rectangular metallic loop featuring a narrow gap between each ring. Due to the gap that prevents current flow, the LC circuit becomes more resonant. The inductive and capacitive reactance must be of equal amplitude for resonance to occur (A Nadin. and M. I. Hussein, 2020). Sensors can be made with SRR because the space acts as a capacitor (A Nadin. and M. I. Hussein, 2020). As shown in Figure 1, W_1 is used to excite the sensor, which produces dual-band responses of 2.5 GHz and 6.5 GHz. 7 GHz.

In this sensor, the top layer of the substrate is carved from an FR4 material that measures 1.6 mm in thickness, possesses a relative permittivity of 4.3, and has a loss tangent of 0.025. CST and ADS were used to optimize and validate the sensor performance. According to Table 1, The proposed sensor has the following optimal parameters.

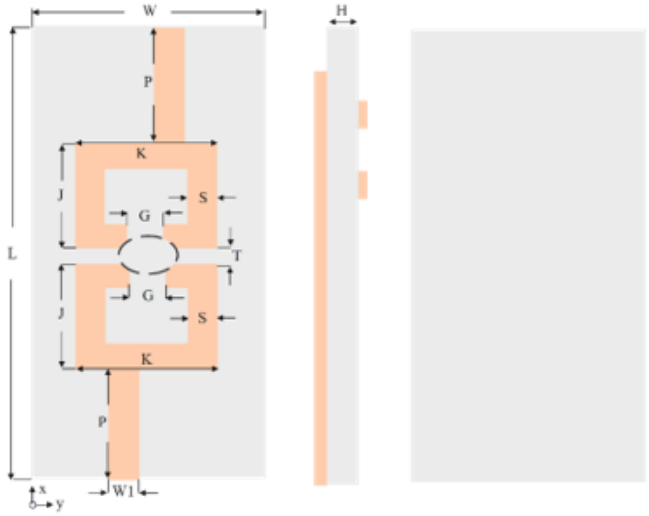

Figure 1: The proposed microwave sensor structure (a) Front view, (b) side view, (c) Back view

Table 1: Optimized sensor design geometry

Parameters	Value (mm)	Parameters	Value (mm)
G	2	P	18
H	1.6	S	2.8
J	14	T	4
K	10	W	20
L	60	W_1	3.1

A. Evolution Steps

As shown in Figure 2(a), several procedures should be followed in order to complete the development of a microwave sensor. In terms of frequency range, the MTM MIMO antenna can operate anywhere from 1 to 7 GHz as the frequency range. According to Figure 2(b), sensor I's S_{11} response does not meet expectations due to the port's position. Shifting the feedline sideways further enhances the dual-band characteristics of the S_{11} response. The third phase of the proposed sensor involved the incorporation of an additional element and an appropriate adjustment of the feeding port. This revised configuration improves the sensor's performance regarding impedance matching. The variation in design parameters, such as resonator width (w), gap capacitance (G), and the substrate's permittivity value, leads to changes in the transmission coefficient (S_{11}) and f_r. The sensor resonator's width influences the total inductance, which in turn affects the resonance frequency. Modifying the width of the resonator is crucial for adjusting the inductance value, directly impacting the relative frequency of the metamaterial. The primary purpose of incorporating a split gap in the metamaterial resonator is to change the sensor's resonance frequency, as this divided gap introduces capacitance that directly affects the resonance frequency. Consequently, the capacitance resulting from the gap is vital for altering the capacitance value, which consequently has a direct effect on the resonant frequency, f_r. Additionally, the permittivity (ε_r) of the substrate material influences the resonant frequency since it is associated with capacitance. Therefore, the design parameters were evaluated to enhance the proposed sensor.

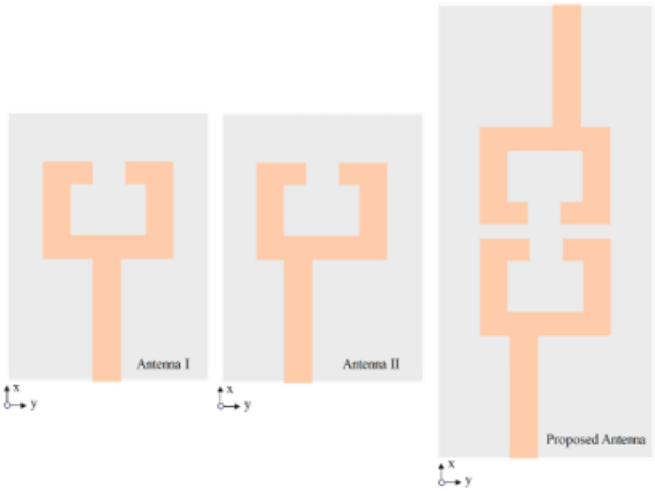

(a)

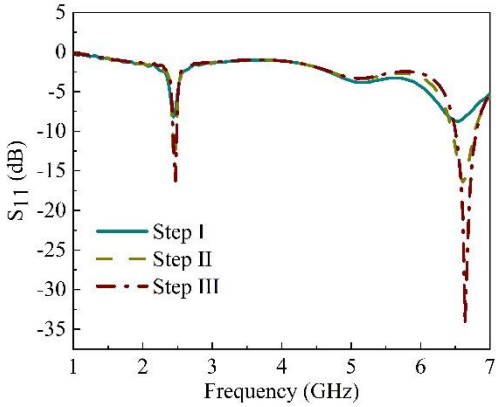

(b)

Figure 2: (a) Evolution stages of the proposed microwave sensor, (b) S_{11} response of the various stages.

Figure 3 demonstrates the influence of resonator width on both the f_r and the return loss (S_{11}). The analysis is conducted for resonator widths of 5.24, 5.28, 5.36, 5.4, and 6mm. The main impact of introducing a resonator into a metamaterial resonator patch is the alteration of the sensor's resonance frequency. This is one of the significant effects observed. Table 2 presents the changes in f_r and S_{11} associated with the different resonator widths. According to Table 2, the 5.36 mm

resonator width demonstrates superior performance compared to the others, leading to the selection of 5.36 mm as the resonator width.

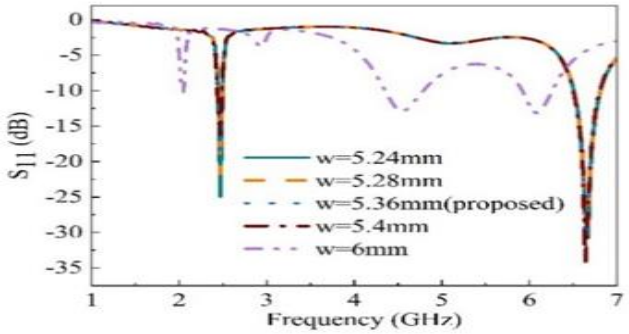

Figure 3: Variation of frequency and S_{11} magnitude for resonator width (w).

Table 2: The effect of the resonator width (w) on the frequency (f_r) and S_{11} amplitude for the frequency range, 1 – 7 GHz.

Resonance width (w) mm	f_r (GHz)	S_{11} amplitude (dB)
5.24	2.45, 6.7	-25, -32
5.28	2.49, 6.6	-23, -30
5.36 (proposed)	2.5, 6.5	-19, -34
5.4	2.51, 6.75	-16, -34
6	2, 4.5, 6	-11, -12, -12

Figure 4 shows how the gap capacitance distance (G) influences the resonant frequency (f_r) and return loss (S_{11}). The results were calculated for split gaps of 1 mm, 2 mm, 2.4 mm, 2.8 mm, and 3.2 mm, corresponding to five different resonator configurations. Table 3 illustrates the variations in f_r and S_{11} with the various split gaps. From Table 3, it is evident that the 2 mm split gap outperforms the others, resulting in the choice of 2 mm as the ideal split gap. Figure 5 demonstrates the effect of substrate permittivity (ε_r) on f_r and S_{11}, with a proposed value of 4.3. The results were assessed for permittivity values of 3.26, 3.46, 3.66, 3.77, and 4.3. Table 4 presents the variations of f_r and S_{11} based on these different permittivity values. From Table 4, it is evident that a permittivity value of 4.3 outperforms the others, making it the preferred choice for substrate permittivity.

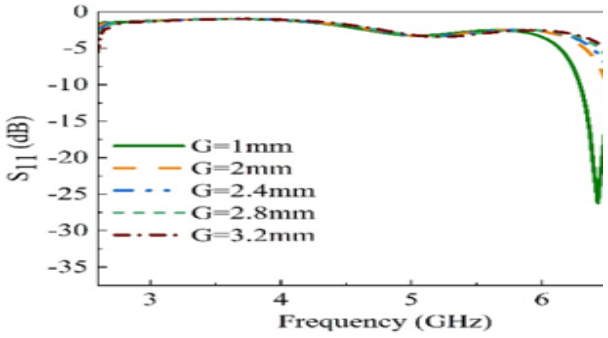

Figure 4: Variation of frequency and S_{11} magnitude for gap capacitance (G).

Table 3: The impact of gap capacitance on the resonance frequency, f_r, and resonance amplitude for the frequency range, 1 – 7 GHz

Gap capacitance distance G (mm)	f_r (GHz)	S_{11} amplitude (dB)
1	2.45, 6.4	-15, -26
2(proposed)	2.5, 6.5	-17, -35
2.4	2.51, 6.75	-16, -30
2.8	2.52, 6.8	-16, -29
3.2	2.53, 6.85	-15, -27

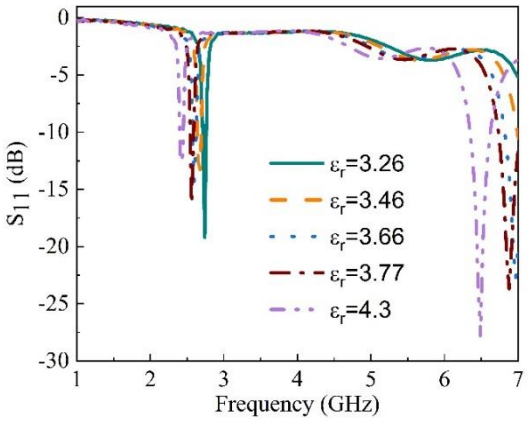

Figure 5: Change in frequency and S_{11} magnitude due to the alteration of the substrate permittivity (ε_r).

Table 4: Effect of substrate permittivity (ε_r) on the resonance frequency and resonance in dB for frequency range, 1 – 7 GHz

Substrate permittivity (ε_r)	f_r (GHz)	S_{11} magnitude (dB)
3.26	2.7, 6.9	-19, -22
3.46	2.6	-18
3.66	2.55, 7	-15, -23
3.77	2.51, 6.85	-16, -23
4.3	2.5, 6.5	-15, -28

B. Equivalent Circuit Model

The parameters of the model are improved through the gradient optimization method, ensuring that the values for each component remain within the specified minimum and maximum limits of 1×10^{-6} to 1.5×10^{6} which is large enough for convergence during the optimization process (Fauri Y., Ahmad S., et al., 2022). Using the ADS software, the equivalent circuit of the suggested sensor was improved, as shown in Figure 6. The model consists of the connections between the first parallel LC circuit of the power line and an inductor on the left side, which means the first port. Two LC circuits follow in series with a second inductor for the second port. Two capacitors, C3 and C4, and an inductor, L3, are placed between the two parallel LC circuits to serve as a

decoupling capacitor between the two sensors. A comparison with the full-wave CST model, which allows for a dual-band frequency response at 2.5 GHz and 6.5 GHz respectively, is highlighted in Figure 7, which represents the graphical representation of S_{11}. Table 5 shows the components of the improved circuit.

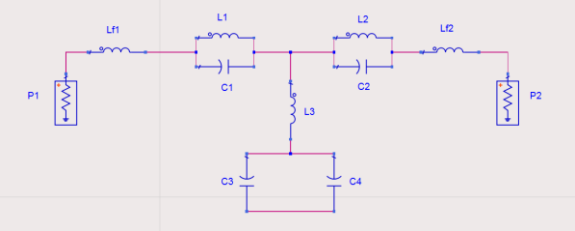

Figure 6: The microwave sensor's equivalent circuit representation.

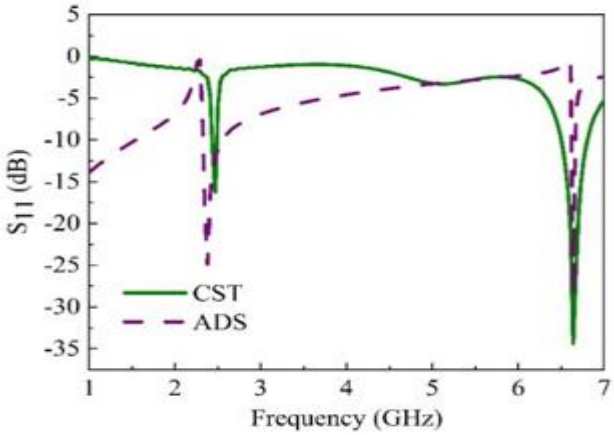

Figure 7: The variation of S_{11} for CST and ADS.

Table 5: Components used for the circuit modelling

C_1 = 1.1433pF	L_1 = 2.065nH	L_{F2} = 772.87pH
C_2 = 470.95fF	L_2 = 1.0947nH	P_1 = 50Ω
C_3 = 0.7626pF	L_3 = 0.6nH	P_2 = 50Ω
C_4 = 0.15pF	L_{F1} = 569.29pH	-

C. Microwave sensor simulated output

The microwave sensor model depicted in Figure 1 simulates the sensor's response by integrating different cell types within the sensor gap. This was accomplished by populating the resonator's gap with representations of breast cancer cells, modelled as hemispherical entities with a diameter of 1 mm. The electrical properties of these malignant breast cells were derived from the research conducted by (D. Jithin, M. I. F. Hussein. Awwad, et al. (2016). Figure 8 shows how the resonance characteristics of air differ from those of the four cell line types (HS578, MCF-7, MDA-MB-231, and MDA-2). For every cell used, the electrical conductivity and dielectric constant are shown in Table 6. One standard is the air's resonance characteristics. Maximum transmission occurs at resonance frequencies of 2.42 GHz. The resonance frequency difference between two adjacent cell types is as small as 0–28 GHz.

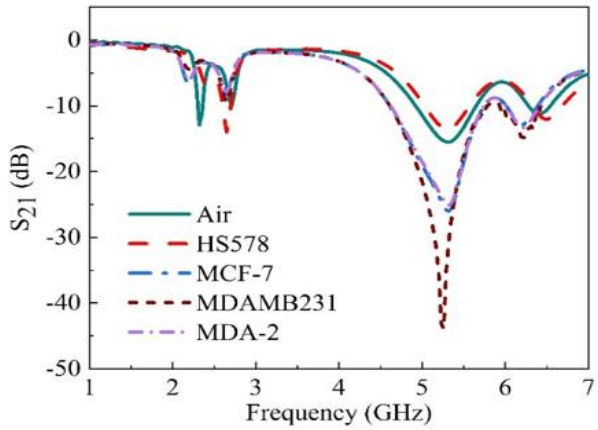

Figure 8: Simulated S_{21} in decibel

Table 6: Dielectric characteristics and the conductivity of the cell

Cancer cell	HS578	MCF-7	MDA-MB-231	MDA-2
Dielectric constant (ε_r)	44.48	42.74	42.24	41.6
Conductivity (σ)	1.479	1.368	1.433	1.656

The shift in resonance frequency of cancerous cells compared to air's resonance frequency is shown in Table 7.

$$\Delta f = f_{cancerouscell} - f_{air} \quad (3)$$

Table 7: The alteration in frequency in relation to the air resonance frequency

Cancer cell	HS578	MCF-7	MDA-MB-231	MDA-2
Shift with respect to air (Δf)	0.28GHz	3GHz	2.83GHz	3.01GHz

D. Measurement procedure

To acquire the sensor response, it is necessary to calibrate the vector network analyzer (VNA) beforehand to remove losses and systematic inaccuracies. The calibration process is the standard process for all microwave devices, and it involves four phases: short, open, load, and through (SOLT). This calibration was executed using two ports to ensure accurate error correction for transmission and reflection in the forward and reverse directions. Different kinds of breast cancer cells have been successfully used to test the proposed sensor. An illustration of the measurement setup can be found in Figure 9. A simulation will be conducted to generate and compare different cancer cell responses. FR-4 laminates, which have a thickness of 1.6 mm and a dielectric constant of 4.3, were used to build the sensor.

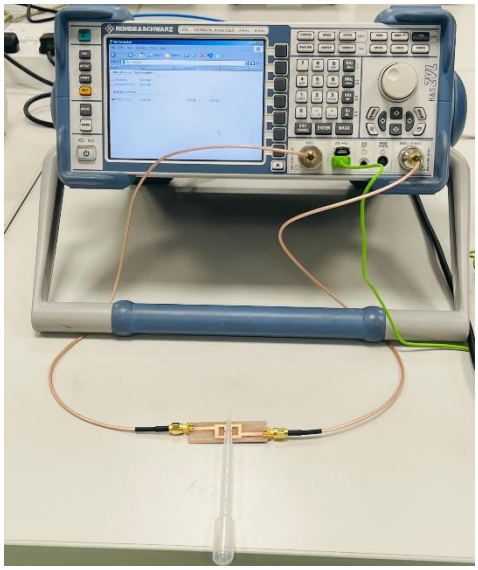

Figure 9: The measurement setup

E. Sensitivity and Quality Factor

The sensitivity of a resonator can be expressed in terms of the change in resonance frequency due to a sample's relative permittivity, as stated in the following equation (W. J. Wu, W. S. Zhao et al., 2021).

$$S = \frac{\Delta f}{\Delta \varepsilon_r} \tag{4}$$

Where Δf is the resonance frequency shift with respect to air, $\Delta \varepsilon_r$ is the variation on the dielectric constant of the breast cancer cells loaded on the microwave sensor structure. The quality factor of the microwave sensor can be expressed by the following formula (W. J. Wu, W. S. Zhao et al., 2021).

$$Q = \frac{2f_r}{\Delta f} \tag{5}$$

Where f_r is the resonance frequency of the sample under test, and Δf is the frequency bandwidth of the resonant peak at -3 dB, with Q being the quality factor.

IV. RESULTS AND DISCUSSION

Figure 10 shows the printed prototype that has been etched using the standard etching machine. Air surrounds the sensor because of the way it is positioned. A micropipette was used to deposit the cells into the gap. The sensor was exposed to two drops, forming a hemispherical droplet with a 1 mm diameter. The sensor was cleaned with ethanol after each sample was measured, and an air pump was used to let it dry. During the measurement, four kinds of cancer cells were examined: MCF-7, MDA-MB-231, MDA-2, and HS578. The S_{21} parameters were acquired and recorded in each instance.

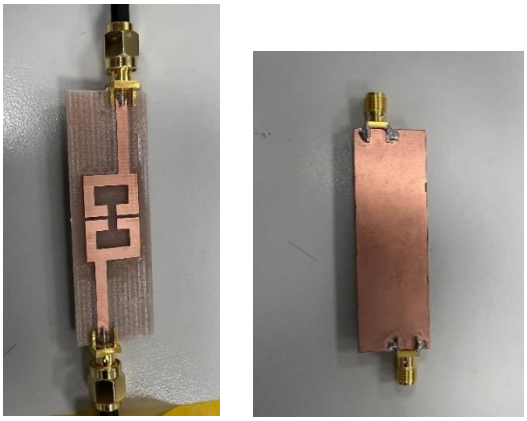

(a) (b)

Figure 10. Prototype views of the Microwave sensor (a) Upper plane (b) Lower plane

The graph in Figure 11 shows the simulated and measured reflection coefficient (S_{11}) when the microwave sensor is not in contact with the material under test (MUT). The simulated resonance frequencies are 2.3, 5.3 and 6.4 GHz with S_{11} magnitude of -12.6, -15.2, and -11.2 dB, where the measured f_r is 2.6, 5.32, and 6.48GHz with S_{11} magnitude of –14, -13 and -12 dB. The results of measuring the resonance characteristics of HS578, MCF-7, MDA-MB231, and MDA-2, in comparison to the resonance characteristics of air, are shown in Figure 12. The simulation results are compared with the lab measurements. The air is established as a baseline, and the frequency change for the four distinct cancer cells is determined. A series of measurements of different samples have been established before arriving at the final four cells, as mentioned above. This is done to reduce the challenges encountered during the fabrication and measurement process.

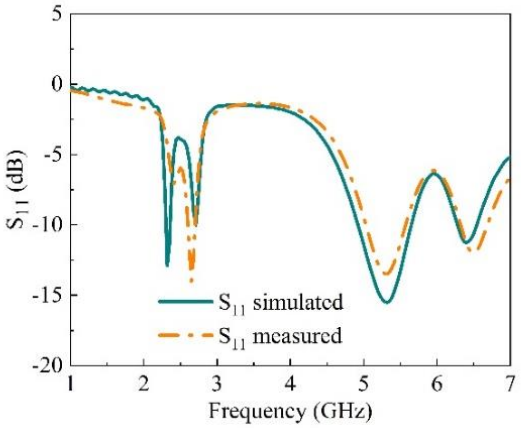

Figure 11: S_{11} responds when the sensing materials are not in contact with the sensor

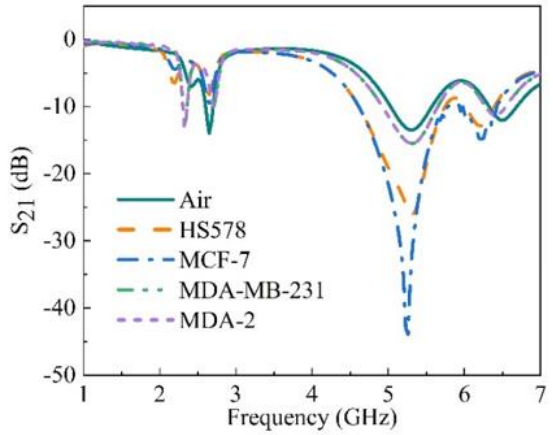

Figure 12: Measured S_{21} in decibels

Figures 13 and 14 show the comparison. The discrepancies noted between the simulated and measured values may result from calibration and manufacturing errors, and this can be reduced by taking at least two to three times the calibration process. The highest shift achieved between the simulation and the measurement is 0.1 GHz. Table 8 presents a summary of the recorded values and the variation in the frequency response of the four cells in relation to the air resonance frequency. The integration of artificial intelligence and machine learning models in the future will further help in rapid and accurate classification.

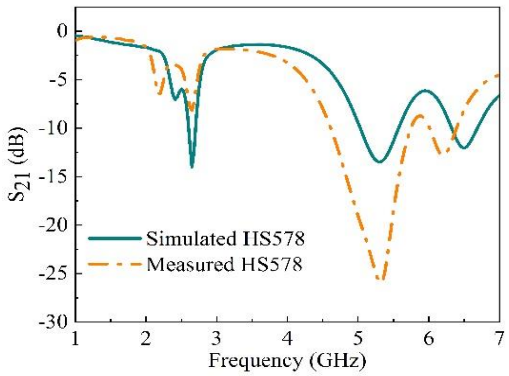

(a)

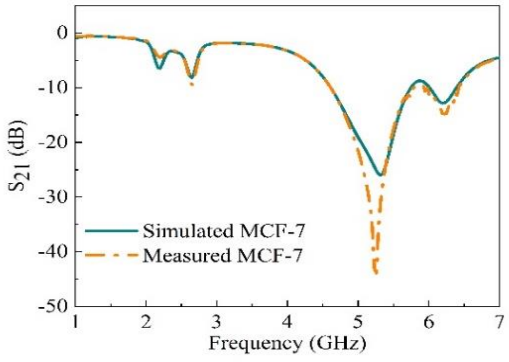

(b)

Figure 13: Measured and simulated S_{21} of (a) HS578 cell, (b) MCF-7 cell

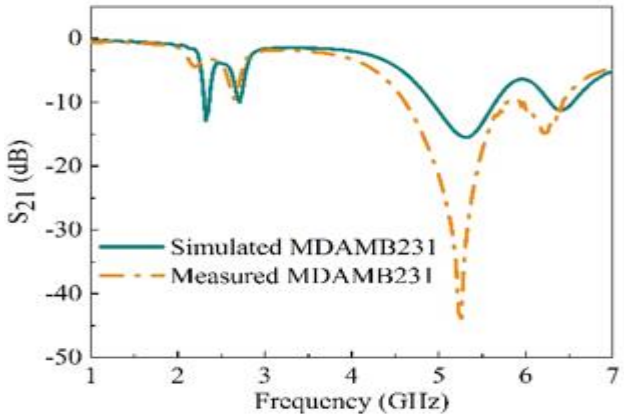

(a)

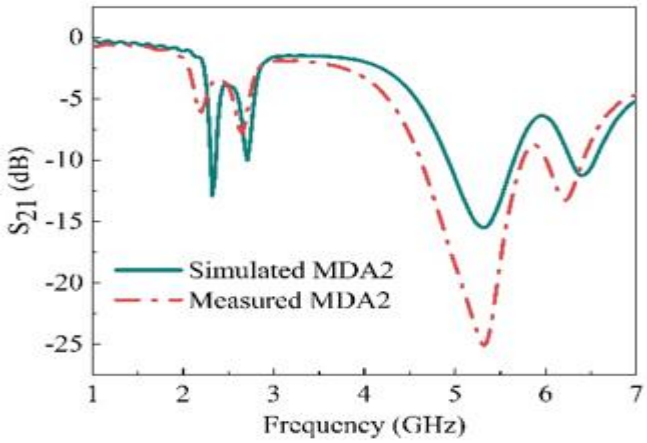

(b)

Figure 14: Measured and simulated S_{21} of (a) MDA-MB-231 cell, (b) MDA-2 cell

Table 8: Lab measurement results

Cancer cell	HS578	MCF-7	MDA-MB-231	MDA-2
Frequency (GHz)	2.81	5.25	5.2	5.3
Δf	0.29	2.73	2.68	2.78

The microwave sensor attained a peak relative sensitivity of 0.105. The sensitivity of each of the four cells, measured using air as a reference, was 0.012 for HS578, 0.105 for MCF-7, 0.101 for MDA-MB-231, and 0.102 for MDA-2. However, the quality factor of each of the four cancer cells was calculated according to equation 5, which is mentioned above. The estimated values of both equations (4) and (5) are shown in Table 9. The microwave sensor has the highest relative quality factor of 16.1.

Table 9: Sensitivity and quality factor results for the proposed microwave sensor using air as a reference

Cancer cell	HS578	MCF-7	MDA-MB-231	MDA-2
$S = \frac{\Delta f}{\Delta \varepsilon_r}$	0.012	0.105	0.101	0.102
$Q = \frac{2f_r}{\Delta f}$	16.1	5.3	9	7.1

The sensor's performance has been evaluated in relation to recent studies published in the literature, as presented in Table 10. Taking into account the sensing range, the suggested sensor's sensitivity is determined to be greater than that documented in existing studies.

Table 10. Comparison of the proposed sensor's sensitivity with state of art

Ref.	$f_{unloaded}$ (GHz)	Sensitivity (%)	Substrate used
[25]	5.112	3.27	RT Duroid 4003C
[28]	3.364	4.915	Taconic TLY-5
[29]	2.65	1.23	Rogers 4350B
[30]	2.1	3.4	Rogers R0 4350
[32]	2.23	0.737	RT Duroid 4350
This work	**2.5, 6.7**	**1.2, 10.5, 10.1, 10.2**	**FR-4**

V. CONCLUSION

In this research, a biosensor utilizing metamaterial technology to examine different types of cancer cells based on their electrical characteristics is presented. The proposed sensor features a double split ring resonator (SRR) integrated into a two-port rectangular microstrip-fed grounded planar configuration. The performance of the sensor is simulated and assessed using four types of cancer cells: HS578, MCF-7, MDA-MB-231, and MDA-2, along with air serving as a vacuum. The sensor exhibits strong sensing capabilities across a frequency range of 1 GHz to 7 GHz. In the future, this concept will be combined with supplementary elements to develop an autonomous device that not only enhances its functionality but also increases its adaptability to various environments and tasks. By integrating advanced technologies such as artificial intelligence and machine learning models, the device could learn from its surroundings and improve its performance in terms of rapid and accurate classification for clinical translation.

AUTHOR CONTRIBUTIONS

A. H. Jabire: Conceptualization, **M. I. Hussein, S. Saminu:** Methodology, **A. H. Jabire. M. I. Hussein:** Software, **A. H. Jabire., S. Saminu., and A. S. Muhammad:** Validation, **A. A. Owoade, S. Saminu., and D. A. Ariyoosu:** formal analysis, **S. Saminu., and A. S. Muhammad:** investigation, **A. A. Owoade, and D. A. Ariyoosu:** writing-original draft preparation, **A. H. Jabire., S. Saminu., and M. J Adamu:** writing review and editing, **A. A. Owoade, A. S. Muhammad, and D. A. Ariyoosu:** visualization, **A.H. Jabire and M. J. Adamu:** Supervision, **M. I. Hussein and M. J. Adamu**: project administration **A. H. Jabire, and M. I. Hussein:** funding acquisition, **A. H. Jabire.**

ACKNOWLEDGEMENT(S)

The author would like to acknowledge the Tertiary Education Trust Fund (TETFUND) Taraba State University chapter for its support and funding.

REFERENCES

A. Buragohan, A. T. T. Mostako, and G. S. Das (2021). Lowcost CSRR based sensor for determination of dielectric constant of liquid samples, IEEE Sensors J., 21 (24): Art no 24.

A. Ebrahimi, J. Scott, and K. Ghorbani, (2018). Differential sensor using microstrip lines loaded with two split ring resonator, IEEE Sensors J. 18 (14): 5780-5793.

A. H. Jabire, A. Ghaffar, Y. Faouri, (2024). Frequency and pattern reconfigurable CPW-Fed MIMO antenna with multiband and wideband characteristics, IEEE Access, 12, 120165-120180.

C. G. Juan, E.Bronchalo, B. Potelon, et al., (2019). Concentration measurement of microliter volume glucose solution using Q factor of microwave sensors, IEEE Trans. Instrum. Meas., 68 (9):

D. Jithin, M. I. Hussein, F. Awwad, and R. Irtini, (2016). Dielectric characterization of breast cancer cell lines using microwave, In proc. ICEDSA Ras Alkhaimah, 1-4.

D. M. Pozar, (2017). Microwave Engineering 4th Edition, New Delhi, Wiley India.

E. L. Chuma and T. Rasmussen, (2022). Metamaterial-based sensor integrating microwave dielectric and near-infrared spectroscopy technique for substrate evaluation, IEEE Sensors J. 22, 19308.

E. L. Chuma, Y. Iano, L. L. B. Roger et al. (2022). Novelty sensor for detection of wear particles in oil using integrated microwave metamaterial resonator with neodymium magnets, IEEE Sensors J., 22, 10508.

E. L. Chuma, Y. Lano, G. Fontgalland, and L. L. B. Roger, (2018): Microwave sensor for liquid dielectric characterization based on metamaterial complementary split ring resonator, IEEE Sensors J. 18 (24): 9978-9983.

Fauri Y. Ahmad S. Naseer S. Alhammami K., et al. (2022). Compact super-wideband frequency diversity hexagonal shaped monopole antenna with switchable rejection band," IEEE Access, 10, 42321-42333.

G. Juan, E. Bronchalo, B. Potelon, C. Quendo, E. Avila-Navarro, and J. M. Sabater-Navarro (2019). Concentration measurement of microliter-volume water–glucose solutions using Q factor of microwave sensors, IEEE Trans. Instrum. Meas., 68 (7): 621–634.

G. Galindo-Romera, J. Carnerero-Cano, J. Martínez-Martínez, and F. Herraiz-Martínez, (2017). An IoT reader for wireless passive electromagnetic sensors, Sensors, 17 (4): p. 693.

G. Ggugliandolo, G. Vermiglio, G. Cutioneo, et al. (2023). Development, characterization and circuit modeling of inkjet printer couple ring resonator for application in biological samples, IEEE Trans. Instrum. Meas., 72, 1.

Hong X. San Y. Cheng G and Juan C, (2022). A dual scale CSRRs based sensor for dielectric characterization of solid materials, IEEE Sensor Letters, vol. 6 (12), 3502704, 2022.

J. Carnerero-Cano, G. Galindo-Romera, J. J. Martinez-Martinez, and F. J. Herraiz-Martinez, (2018). A contactless dielectric constant sensing system based on a split-ring resonator-loaded monopole, IEEE Sensors J., 18 (11): 4491–4502.

J. K. Park, C. Jang, G. H. Yun, et al., (2020). Sensitive relative humidity monitoring sensor based on microwave active resonator, IEEE Access, 8: 166283-166293.

J. Naqui and F. Martin, (2014). Angular displacement and velocity sensor based on electric LC (ELC) loaded microstrip lines, IEEE Sensors J. 14 (4): 939-840.

K. Masrakin, S. Z. Ibrahim, H. A. Rahim, et al., (2023). Microstrip sensor based on ring resonator coupled with double square split ring resonator for solid material permittivity characterization, Micromachines, 14 (4): 790.

K. T. Muhammad Shafi, A.K. Jha and M. J. Akhtar, (2017). Improved planar resonant RF sensor for retrieval of permittivity and permeability of materials, IEEE Sensors J. 17 (7), 5479-5486.

M. A. H. Ansari, A. K. Jha, and M. J. Akhtar, (2015). Design and application of CSRR based planar sensor for noninvasive measurement of complex permittivity, IEEE Sensors J. 15 (12): 7181-7189.

M. I. Hussein, F. Awwad, D. Jithin, H. El Hasasna, K. Athamneh and R. Iratni (2019). Characterization of breast cancer-specific dielectric signature in vitro using the open-ended coaxial probe technique from 200 MHz to 13.6 GHz. Scientific Reports, 9 (1): 4681.

M. S. Boybay, and O. M. Ramahi, (2012). Material characterization using complementary split ring resonator, IEEE Trans. Instrum. Meas. 61 (11), 3039-3046.

M. U. Memon, A. Salim, H. Jeong, and S. Lim, (2020). IEEE Trans. Instrum. Meas., 69 (4), 1344-1352.

P. K. Varshney, A. Kapoor, and M. J Akhtar, (2021). Highly sensitive ELC resonator based differential sensor, IEEE Trans. Instrum. Meas. 70 1-10.

P. K. Varshney, A. Sharma and M. J. Akhtar, (2020). Exploration of adulteration in some food materials using high sensitivity configuration of electric LC resonator sensor, Int. J. RF Microw Comput Aided Eng., 30 (2): 22045.

P. Yazhmaee and H. Minoofar, (2014). Electric LC resonator as a microwave for oil sensing, Electronic Letters, 50 (16): 1147-1148

R. Yadav and P. N. Patel (2018). Characterization of high-frequency dielectric laminates using a scanning probe based on EBG structure. IEEE Trans. Instrum. Meas. 67 (1): 107–115.

S. Jiang, G. Liu, M. Wang, Y. Wu and J. Zhou, (2023). Design of high sensitivity microfluidic sensor based on CSRR with interdigital structure, IEEE Sensors J., 1-1.

W. J. Wu, W. S. Zhao, D. W. Wang et al. (2021). A temperature compensated differential microstrip sensor for microfluidic applications, IEEE Sensors J. 21 (21): 24075 – 24083.

W. S. U., B. S. Cook, and M. M. Tentzens, (2016). Additively manufactured microfluidic based peel and replace RF sensor for wearable applications, IEEE Trans. Microw. Theory and Techn., 64 (6): 1928-1936.

W. Withayachumnankul, K. Jaruwongrungsee, A. Tuantranont, et al., (2013). Metamaterial based microfluidic sensor for dielectric characterization, Sensors and Actuators A: Physical, 189, 233-237.

Xinyue Song, Sen Yan and Juan Chen, (2023). A design of metamaterial inspired resonator for multi-frequency fluidic sensors, IEEE Microw. Wirel. Tech. Lett., 33(1): 94–97.